CHAPTER IV

RESULTS AND DISCUSSIONS

4.1 Morphology of TiO_2 nanofibers

TiO_2 nanofibers were fabricated via electrospinning process. The following parameters have been varied to obtain the nanometer range of fibers.

4.1.1 Effect of polyvinylpyrrolidone (PVP) content in TiO_2 electrospinning solution

At first, the TiO_2 electrospinning solution was prepared by mixing 43% (w/w) of titanium isopropoxide, 43% (w/w) of 2-butanone, PVP at 11% (w/w), 1% (w/w) of *N,N'*-dimethylformamide, and 2% (w/w) of ethanol [30]. Parameter of PVP content was studied by varying the amount of PVP at 3%, 6%, 11%, and 16% (w/w), respectively. At 16% (w/w) of PVP content it was found that the mixture coagulated into a gel-liked form. However, the mixture can be dissolved into homogeneous solutions at lower PVP contents. For this preliminary research, electrospinning condition was fixed at 18 kV voltage, a 20 cm distance from needle tip to collector, 1.2 mL/h of feeding rate [62], and needle diameter used was at 0.9 mm. After an hour, the electrospun PVP-TiO_2 fibers were obtained as white sheets. Morphology of the PVP-TiO_2 fibers were investigated by SEM, as shown in **Figure 4.1**.

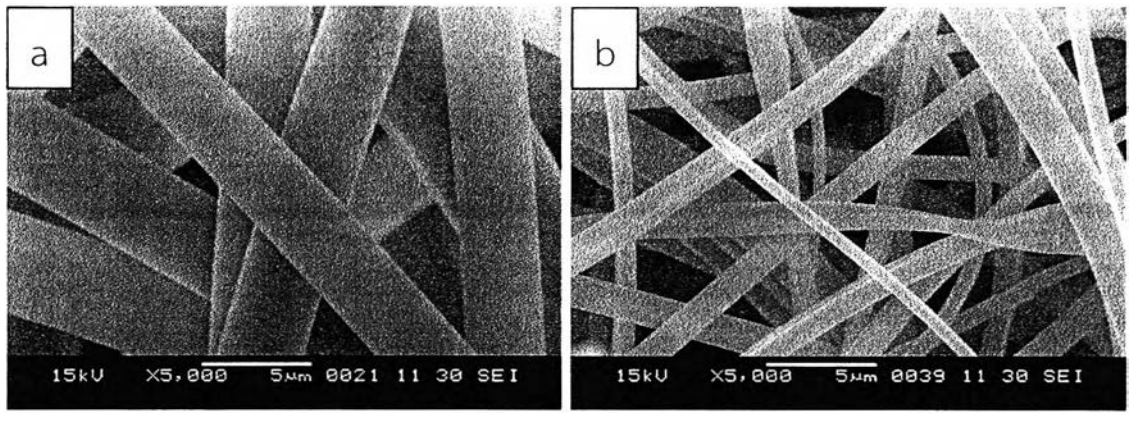

Figure 4.1 PVP-TiO_2 fibers a) at 11% (w/w) and b) at 6% (w/w) g of PVP content

Table 4.1 Diameter of PVP-TiO_2 fibers at 0.4 and 0.8 g of PVP content

PVP content (%(w/w))	Diameter of PVP-TiO_2 fibers (μm)
6	1.34±0.42
11	4.21±0.62

It has been observed from SEM micrographs that diameters of PVP-TiO_2 fibers increased with increasing PVP content. This result is agree well with previous reports [24, 55, 70]. It can be seen that at 6% (w/w) of PVP content, the PVP-TiO_2 fibers were obtained in 0.92-1.76 μm diameter range. Hence, 6% (w/w) of PVP content was selected to be the condition for electrospinning. In addition, decreasing PVP content to 3% (w/w) resulted in failure in fiber formation.

4.1.2 Effect of titanium isopropoxide content in TiO_2 electrospinning solution

From the starting condition of PVP at 11% (w/w) [30], parameter of titanium isopropoxide content was studied along with PVP content. Titanium isopropoxide was varied between 14% and 57% (w/w) in electrospinning solution which after combining with 2-butanone make up to 6 g of solution. For example, 3 g of titanium isopropoxide was mixed with 3 g of 2-butanone. At 14% (w/w) of titanium isopropoxide content, fibers were not obtained. Nonetheless, increasing of titanium isopropoxide content to 28% (w/w) enabled the fabrication to be successful. The fibers were subjected to SEM analysis. Morphology of fibers at 28% to 57% (w/w) of titanium isopropoxide content are shown in **Figure 4.2** and **Table 4.2**.

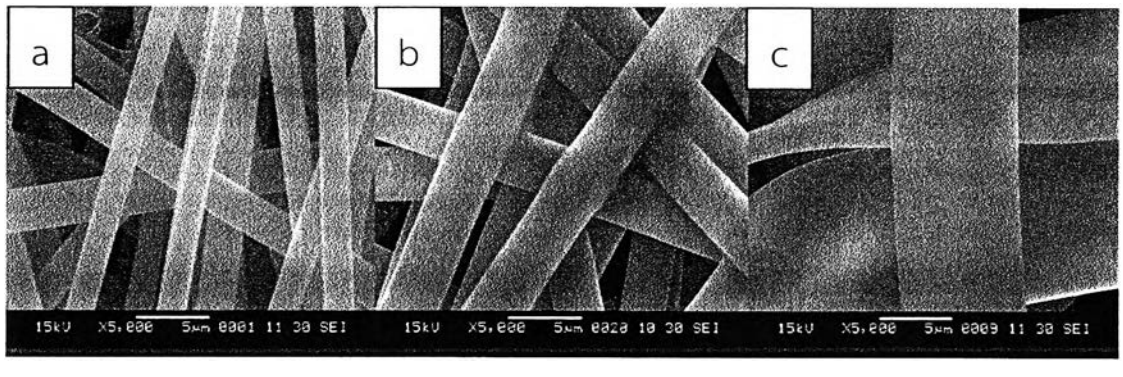

Figure 4.2 Morphology of PVP-TiO_2 fibers at a) 28%, b) 43%, and c) 57% (w/w) of titanium isopropoxide content

Table 4.2 Diameter of PVP-TiO_2 fibers at 28%, 43%, and 57% (w/w) of titanium isopropoxide content

Titanium isopropoxide content (%(w/w))	Diameter of PVP-TiO_2 fibers (μm)
28	2.05±0.19
43	4.21±0.62
57	9.28±1.52

The SEM micrographs exhibited that an increase in PVP-TiO_2 fibers diameter was observed when the titanium isopropoxide content increased. This result also conforms to other previous reports [55, 71]. From preliminary research, the diameter of PVP-TiO_2 fibers is larger than the expected size (500-1,000 nm range). Therefore, such parameters have to be adjusted in order to obtain fibers with the diameter in nanometers. Needle size was changed from 0.9 mm to 0.4 mm. Heikkilä *et al.* [57] reported that decreasing of needle size causes the decreasing of diameter of fibers. Titanium isopropoxide content was adjusted to 23% (w/w). Also the PVP content was selected at 6% (w/w). PVP-TiO_2 fibers have been found that decreasing in diameters (1.22±0.41 μm) when compared with **Figure 4.2**, as shown in **Figure 4.3**.

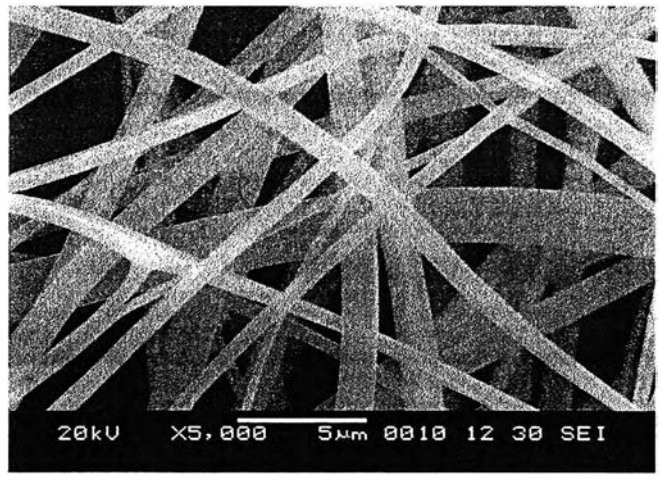

Figure 4.3 Fabricated PVP-TiO_2 fibers at 18 kV of voltages, 1.2 mL/h of feeding rate, 20 cm of distances between needle tip and collector, 23% (w/w) of titanium isopropoxide, 6% (w/w) of PVP, and 0.4 mm of needle size

4.1.3 Parameters of electrospinning method

Parameters such as voltages, distances from needle tip to collector, and the feeding rate were also studied to obtain optimized conditions to fabricate the desired nanofibers.

4.1.3.1 Effect of feeding rate on fiber characteristics

Feeding rate of the electrospinning solution was studied at 0.6, 0.9, and 1.2 mL/h. Diameters of the obtained PVP-TiO_2 fibers fabricated at different feeding rate are shown in **Figure 4.4** and the data summarized in **Table 4.3**.

Table 4.3 Diameter of PVP-TiO_2 fibers at 0.6, 0.9, and 1.2 mL/h of feeding rate (18 kV and 20 cm)

Feeding rate (mL/h)	Diameter of PVP-TiO_2 fibers (μm)
0.6	0.89±0.20
0.9	0.96±0.38
1.2	1.22±0.41

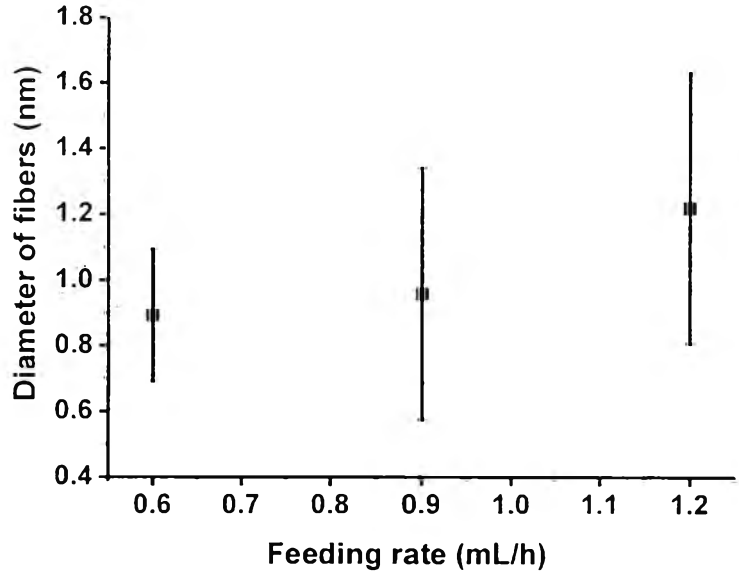

Figure 4.4 Diameter of PVP-TiO_2 fibers at feeding rate of 0.6, 0.9, and 1.2 mL/h (18 kV and 20 cm)

At 0.6 mL/h of feeding rate, it has been found that the average diameter of PVP-TiO_2 fibers is lower than that at obtained at the higher feeding rate. In addition, there were

less distribution of fibers size than fibers prepared under other conditions. Moreover, diameter of fibers is in the range of micro- to nanometers.

4.1.3.2 Effect of distances from needle tip to collector on fiber characteristics

Distances from needle tip to collector was studied at 20, 25, and 30 cm in order to get an appropriate distance for fabrication. This effect is exhibited in **Table 4.4** and **Figure 4.5**.

Table 4.4 Diameter of PVP-TiO_2 fibers at distances from needle tip to collector of 20, 25, and 30 cm (18 kV and 0.6 mL/h)

Distance from needle tip to collector (cm)	Diameter of PVP-TiO_2 fibers (μm)
20	0.89±0.20
25	0.68±0.08
30	0.92±0.44

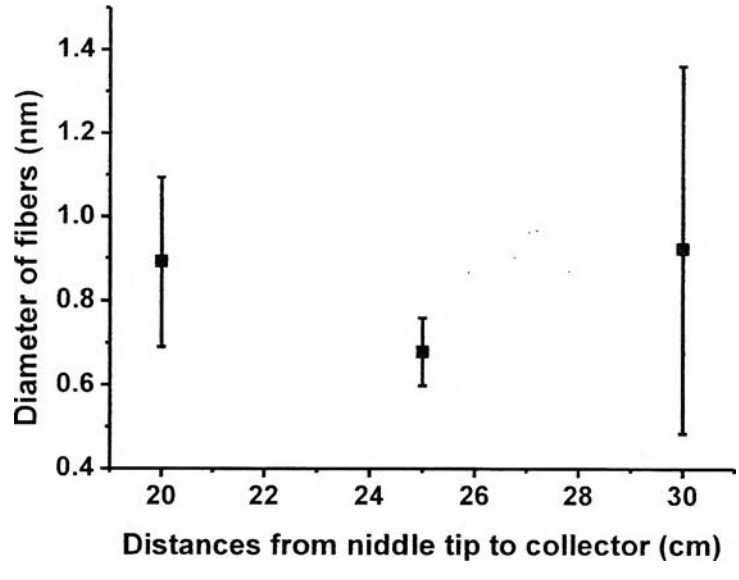

Figure 4.5 Diameter of PVP-TiO_2 fibers at 20, 25, and 30 cm of distances from needle tip to collector (18 kV and 0.6 mL/h)

It can be seen that at 25 cm of distances from needle tip to collector, fibers with the lowest diameter which is about 680 nm was obtained. Nevertheless, more distances from needle tip to collector shows higher diameter size and larger diameter distribution of fibers. There are a few reasons to explain this behavior. First, a larger distances between from tip to collector enhances evaporation of solvent, leading to decrease size of fibers. However, evaporation of solvent depends on relative humidity and volatility of solvent [56, 72]. Relative humidity of the fabrication chamber was about 60-70 % which is quite high. Thus, increasing of distances between needle tip and collector does not increase evaporation of solvent that much and also reduces electric field strength [72-74]. Second, electric field strength is changed when increases distances between needle tip and collector. Electrostatic repulsion is reduced which causes unstable of electrospinning jet, leading to larger fibers and higher distribution. Besides, density of fibers at 30 cm is lower than at 20 and 25 cm, as shown in **Figure 4.6.** Hence, distances from needle tip to collector at 25 cm was selected to fabricate PVP-TiO_2 nanofibers.

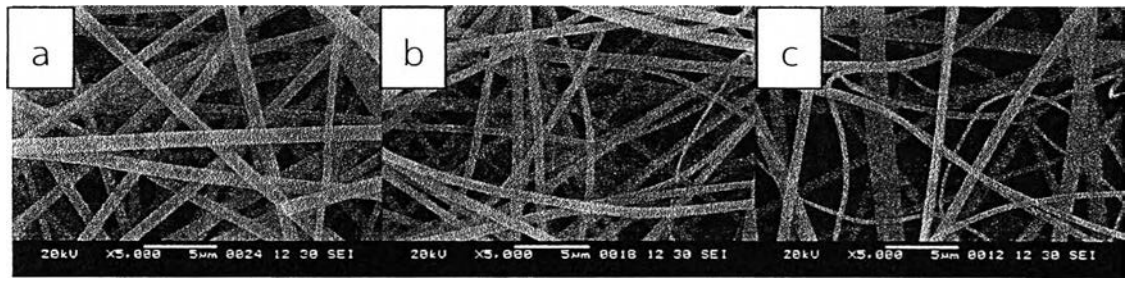

Figure 4.6 Density of PVP-TiO_2 nanofibers at a) 20 cm, b) 25 cm, and c) 30 cm of distances between needle tip and collector (18 kV and 0.6 mL/h)

4.1.3.3 Effect of the applied voltages on fiber characteristics

It is known that high voltages usually results in thin fibers. In this research the applied voltages had been varied in order to find an optimized voltages to be used. Applied voltages in this research were tested at 12, 15, and 18 kV. Analysis on the diameter of fibers is revealed in **Figure 4.7** and the data tabulated in **Table 4.5**.

Table 4.5 Diameter of PVP-TiO_2 fibers at 12, 15, and 18 kV of voltages (25 cm and 0.6 mL/h)

Voltages (kV)	Diameter of PVP-TiO_2 fibers (μm)
12	1.19±0.24
15	0.79±0.23
18	0.68±0.08

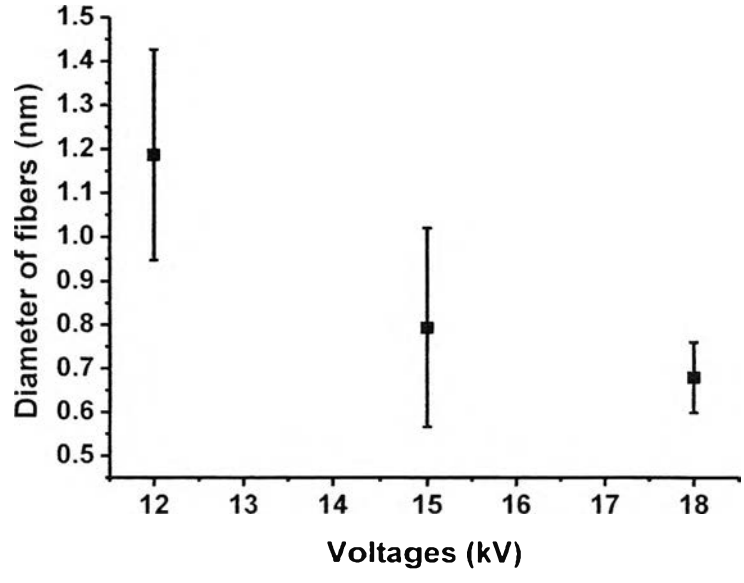

Figure 4.7 Diameter of PVP-TiO_2 fibers at 12, 15, and 18 kV of voltages (25 cm and 0.6 mL/h)

It can be seen that diameter of fibers are inversely proportional to increase voltages as it decreases with increasing voltages. This phenomenon can be found in many reports [50, 56, 57, 70, 75, 76]. Some research groups [56, 57, 70] proposed that higher applied voltages leads to thick fibers due to higher mass flow of the electrospun solution. Thus, at 18 kV of voltages was selected to fabricate PVP-TiO_2 nanofibers.

From the optimization of each parameters used in the electrospinning process, the PVP-TiO_2 nanofibers for gas sensing application were fabricated with a mixtures of 1.5 g of titanium isopropoxide, 4.5 g of 2-butanone, 0.4 g of PVP, 0.1 mL of *N,N'*-dimethylformamide, and 0.2 mL of ethanol electrospinning solution. In addition to electrospinning condition, the optimized parameters of 18 kV of voltages, 25 cm of

distances between needle tip and collector, and 0.6 mL/h of feeding rate were elected to fabricate TiO_2 nanofibers.

Table 4.6 Electrospinning parameters of fabricated PVP-TiO_2 nanofibers

Titanium isopropoxide (g)	1.5
2-butanone (g)	4.5
PVP (g)	0.4
N,N'-dimethylformamide (mL)	0.1
Ethanol (mL)	0.2
Needle size (mm)	0.4
Feeding rate (mL/h)	0.6
Distance from needle tip to collector (cm)	25
Voltages (kV)	18

4.1.4 Hot-pressing followed by calcination of TiO_2 nanofibers

As mentioned earlier, the hot-pressing process has been shown to afford nanofibers with high surface area [8, 23]. Therefore, a hot-pressing process has been carried out here after the electrospun PVP-TiO_2 fibers in desired diameter has been obtained. Hot-pressing process was carried out by using preheated metallic Teflon plate at 180 °C for 10 minutes. This is equal to the glass transition temperature (T_g) of PVP. Subsequently, the calcination was carried out at 600 °C for 1 hour in order to remove all other organic materials. The fibers obtained were subjected to SEM analysis. SEM micrographs show morphology of TiO_2 nanofibers, as smooth uniform fibers as revealed in **Figure 4.8**. As shown in **Figure 4.8 a) and b)**, the average diameter of electrospun PVP-TiO_2 nanofibers and hot-pressed electrospun PVP-TiO_2 nanofibers was observed about 604±167 nm and 578±126 nm respectively. It can be described that electrospun nanofibers were pressed by hot-pressing process, leading to a decrease the diameter of nanofibers. After calcinations step, diameter of both unpressed and hot-pressed electrospun TiO_2 nanofibers decreased because of organic components were removed from TiO_2 nanofibers (**Figure 4.8 c) and d)**). They were found at 484±108 nm for the unpressed electrospun TiO_2 nanofibers and 467±138 nm for the hot-pressed electrospun TiO_2 nanofibers, as indicated in **Table 4.7**.

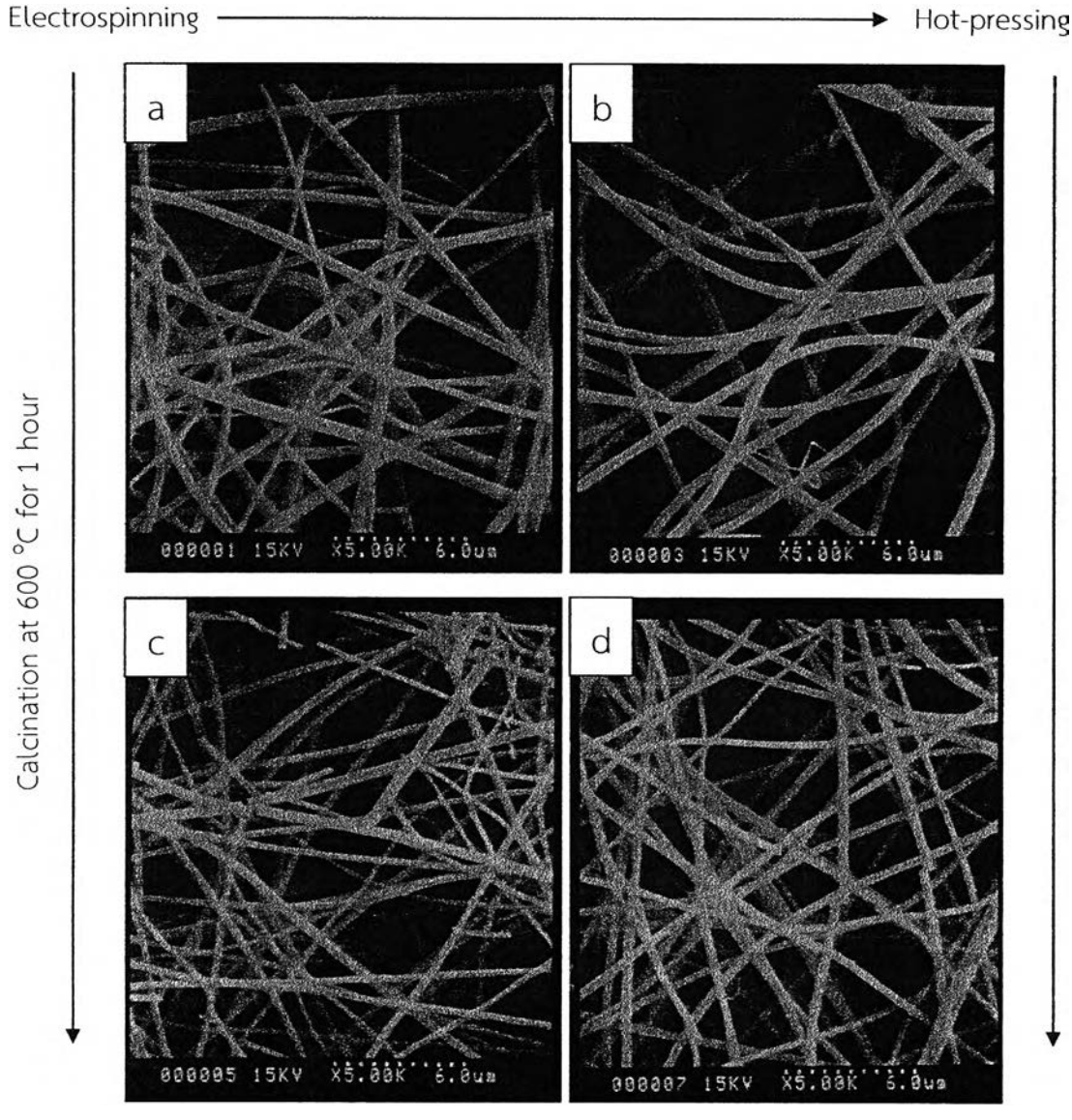

Figure 4.8 SEM micrographs of a) electrospun PVP-TiO_2 nanofibers, b) hot-pressed electrospun PVP-TiO_2 nanofibers, c) calcined electrospun TiO_2 nanofibers, and d) calcined electrospun TiO_2 nanofibers after hot-pressed

Table 4.7 Diameter of electrospun nanofibers at each processing steps

Electrospun nanofibers	Diameter of nanofibers (nm)
a) PVP-TiO_2 nanofibers	604±167
b) Hot-pressed PVP-TiO_2 nanofibers	578±126
c) TiO_2 nanofibers	484±108
d) Hot-pressed TiO_2 nanofibers	467±138

4.2 Crystal structure of sensing materials

After preparation of electrospun nanofibers followed by hot-pressing process and then calcination, the crystal structure of TiO_2 nanofibers were investigated by XRD analysis. In the case of the as calcined TiO_2 nanofibers, peaks of crystal structure of sensing materials are located at 2θ = 25.3°, 27.2°, 36.1°, 36.8°, 37.8°, 38.6°, 48.1°, 54.1°, 54.9°, 62.7°, 69.0°, 70.2°, and 75.4° as shown in **Figure 4.9**.

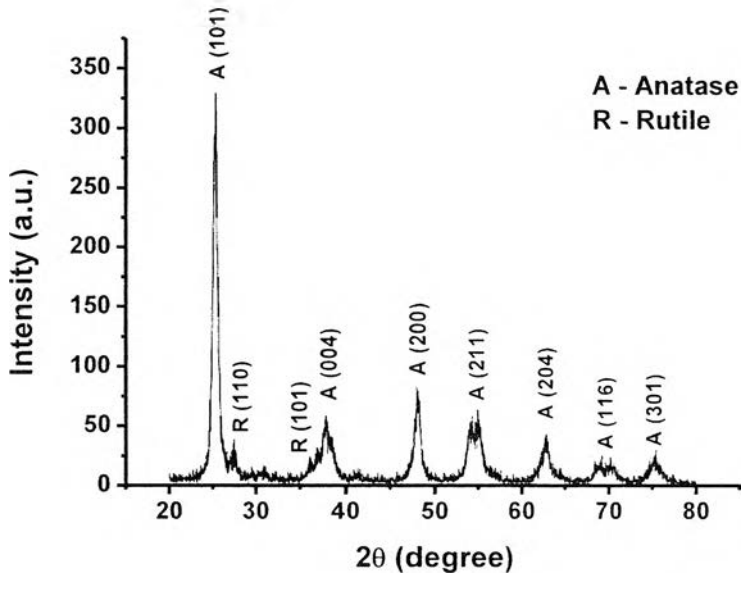

Figure 4.9 XRD pattern of TiO_2 nanofibers as sensing materials calcined at 600 °C for 1 hour

The crystallographic plane of (1 0 1) located at 2θ = 25.3°, (0 0 4) located at 2θ = 36.8°, 37.8°, and 38.6°, (2 0 0) located at 2θ = 48.1°, (2 1 1) located at 2θ = 54.1°, 54.9°, (2 0 4) located at 2θ = 62.7°, (1 1 6) located at 2θ = 69.0° and 70.2°, and (3 0 1) located at 2θ = 75.4° are affirmed the anatase phase whereas crystallographic plane of (1 1 0) and (1 0 1) located at 2θ = 27.2° and 36.1° are the rutile phase [77].

Table 4.8 Crystal structure of obtained TiO_2 nanofibers as sensing materials

Phase	2θ (degree)	Crystallographic plane
Anatase	25.3	(1 0 1)
	36.8, 37.8, 38.6	(0 0 4)
	48.1	(2 0 0)
	54.1, 54.9	(2 1 1)
	62.7	(2 0 4)
	69.0, 70.2	(1 1 6)
	75.4	(3 0 1)
Rutile	27.2	(1 1 0)
	36.1	(1 0 1)

Crystal structure of sensing materials consists of both anatase and rutile while the anatase phase is the main structure. Intensity of XRD pattern also confirmed that anatase phase is the major phase in crystal structure of sensing materials. According to the main peak (1 0 1) located at $2\theta = 25.3^{\circ}$, the grain size of sensing materials is about 15.3 nm. Thus, TiO_2 nanofibers as sensing materials consist of TiO_2 nanocrystalline particles. Besides, calcinations step removed all of the organic components in nanofibers.

4.3 Surface area and contact angle of TiO_2 as sensing materials

In order to investigate the effect of processing method on the properties of the fibers, surface area of both unpressed and hot-pressed electrospun TiO_2 nanofibers were measured via BET analysis. The measured surface area of unpressed electrospun TiO_2 nanofibers is 41.89 m^2/g while hot-pressed electrospun TiO_2 nanofibers is 55.84 m^2/g, as shown in **Figure 4.10**. It can be seen that adsorption isotherm of unpressed and hot-pressed electrospun TiO_2 nanofibers are type IV. The type IV isotherm generally reflects a mesoporous material with average pore diameters between 2 to 50 nm [78, 79]. Average pore diameters of unpressed and hot-pressed electrospun TiO_2 nanofibers is approximately 15 and 16 nm, respectively.

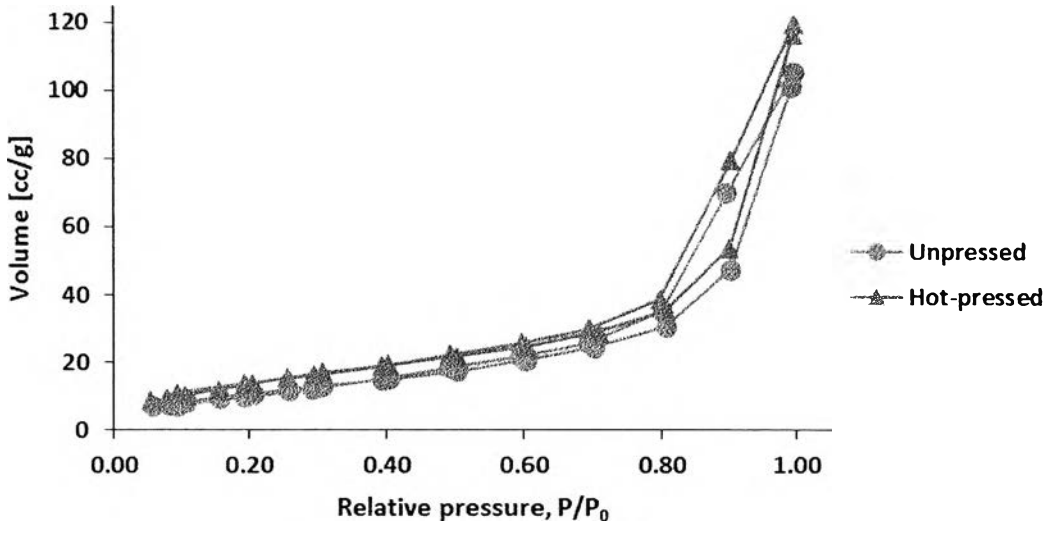

Figure 4.10 Adsorption isotherm of electrospun TiO_2 nanofibers

Hot-pressed electrospun TiO_2 nanofibers exhibits higher surface area. It can be seen that hot-pressing process enhances the surface area of sensing materials which conforms to the reports by Kim *et al.* [8, 23].

Moreover, hot-pressing process also indicates the uniform surface of sensing materials. Contact angle was examined to compare the difference in the fibers obtained with different processing steps. Contact angle of unpressed electrospun TiO_2 nanofibers was in the range of 75-144° while hot-pressed conditions gave materials with contact angle in range 100-150°, as shown in **Table 4.9** and **Figure 4.11**

Table 4.9 Contact angle of unpressed and hot-pressed electrospun TiO_2 nanofibers

Nanofibers	Time (min)	Experiment 1 (degree)	2 (degree)	3 (degree)	4 (degree)	Mean (degree)	SD
Unpressed	0	129.64	144.22	74.77	96.16	111.20	31.54
Hot-pressed	5	147.76	143.45	145.43	109.21	136.47	18.26
	10	144.55	141.25	143.20	140.31	142.32	1.91
	15	140.20	144.89	141.71	99.65	131.61	21.40
	20	136.55	142.72	150.99	143.76	143.50	5.92
	25	143.22	140.60	138.27	135.52	139.40	3.28

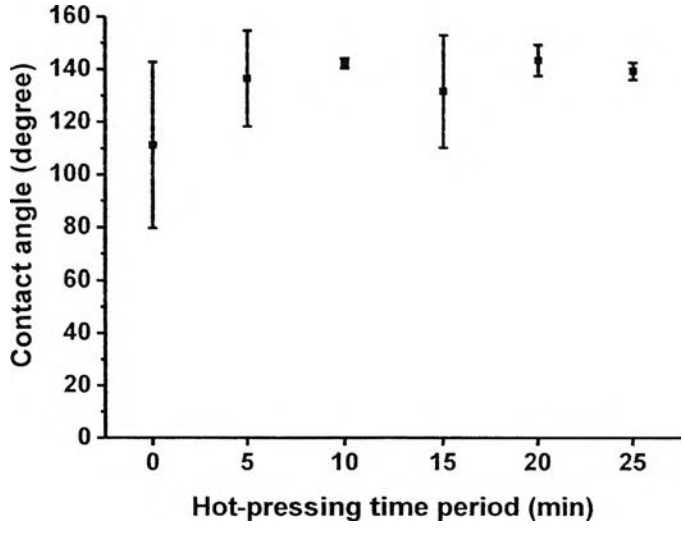

Figure 4.11 Contact angle of unpressed and hot-pressed electrospun TiO_2 nanofibers

For each specimens, after the water droplet was left on the surface of the specimens for 5 minutes, contact angle was measured again to investigate the effect of hot-pressing process to sensing materials surface. Contact angle values of unpressed electrospun TiO_2 nanofibers decrease from 111.20±31.54° to 76.87±63.10° after leaving the water droplet on the specimens' surface for 5 minutes, as shown in **Table 4.10** and **Figure 4.12**. In case of hot-pressing at various time, the hot-pressed electrospun TiO_2 nanofibers at 5 minutes indicates the contact angle values in the same trend with unpressed electrospun TiO_2 nanofibers. It is noteworthy to observe that electrospun TiO_2 nanofibers which were hot-pressed for 10 minutes indicate the similar values of contact angle after leaving the water droplet on the surface for 5 minutes. However, contact angle values of hot-pressed electrospun TiO_2 nanofibers at 15-25 minutes changed from the initial values after leaving the water droplet on the surface for 5 minutes. This may be possible that there are thin nanofibers on the top of surface leading to generate small hole on the surface. The water droplet can diffuse into that hole. Thus, contact angle values decrease.

Table 4.10 Contact angle of unpressed and hot-pressed electrospun TiO_2 nanofibers after leaving for 5 minutes

Nanofibers	Time (min)	Experiment 1 (degree)	2 (degree)	3 (degree)	4 (degree)	Mean (degree)	SD
Unpressed	0	126.40	130.59	-	50.48	76.87	63.10
Hot-pressed	5	15.96	140.20	-	81.22	59.34	64.34
	10	137.77	135.35	141.03	134.71	137.21	2.86
	15	137.43	98.99	130.35	82.39	112.29	26.01
	20	135.21	138.87	138.91	54.08	116.77	41.83
	25	33.30	133.10	133.55	133.73	108.42	50.08

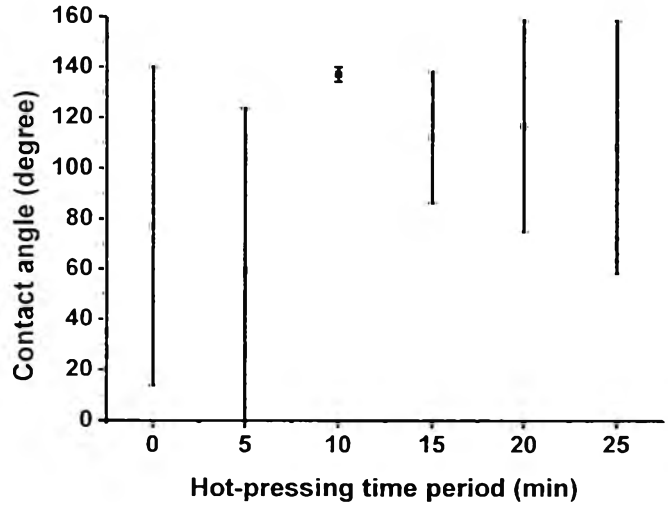

Figure 4.12 Contact angle of unpressed and hot-pressed electrospun TiO_2 nanofibers after leaving for 5 minutes

At initial contact angle measurement, contact angle of both unpressed and hot-pressed electrospun TiO_2 nanofibers was similar (**Figure 4.13 (a) and (c)**). Contact angle values of unpressed electrospun TiO_2 nanofibers decrease which that was observed after leaving the water droplet on the specimens for 5 minutes. It may be considered that surface of unpressed electrospun TiO_2 nanofibers is not uniform (**Figure 4.13 (b)**). Furthermore, hot-pressed electrospun TiO_2 nanofibers at 10 minutes exhibit the same trend after leave for 5 minutes. Hence, it may be considered that hot-pressing process enhances the uniformity of surface materials (**Figure 4.13 (d)**).

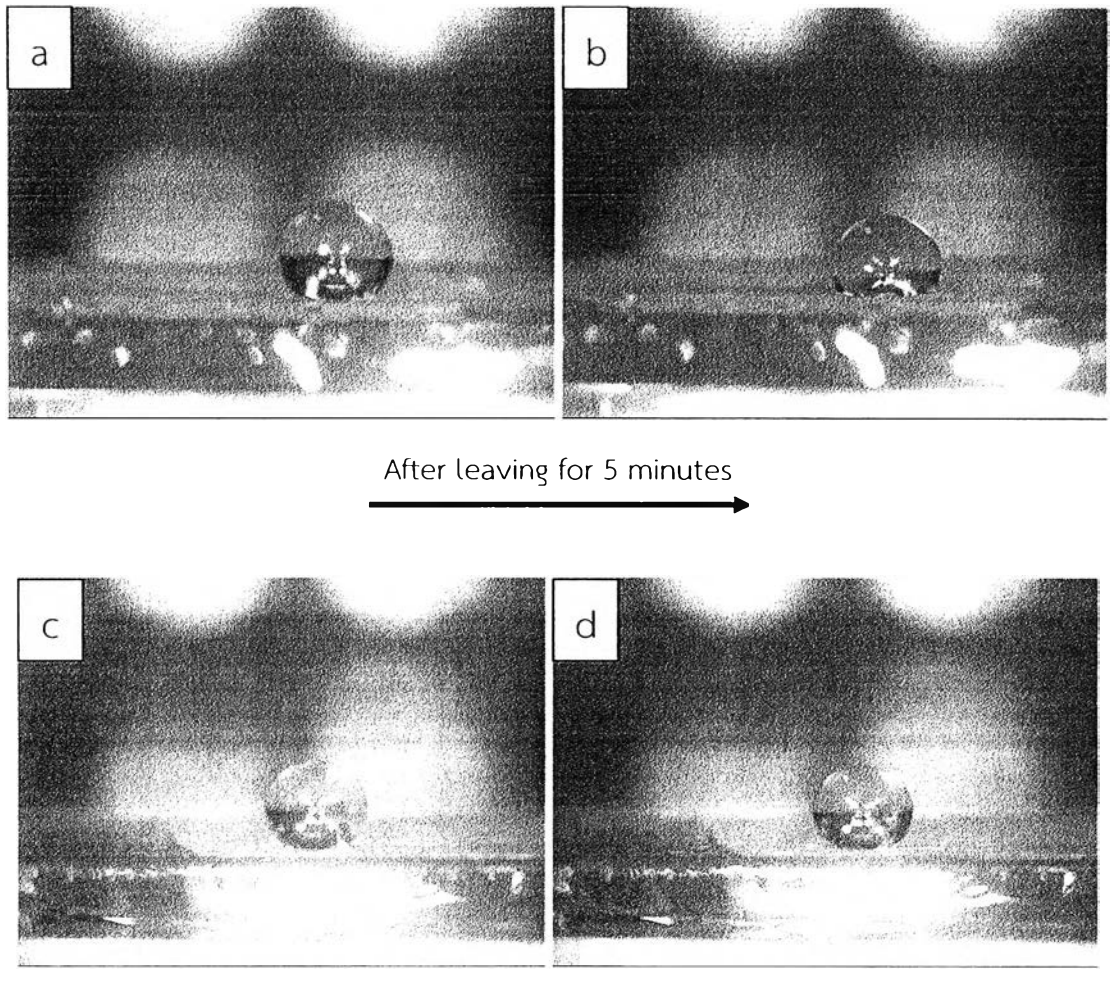

Figure 4.13 A water droplet on a) unpressed electrospun TiO_2 nanofibers, b) unpressed electrospun TiO_2 nanofibers after leaving for 5 minutes, c) hot-pressed electrospun TiO_2 nanofibers at 10 minutes, and d) hot-pressed electrospun TiO_2 nanofibers at 10 minutes after leaving for 5 minutes

4.4 Sensing performance of TiO_2 nanofibers as gas sensor

4.4.1 Gas sensing behavior of TiO_2 nanofiber gas sensor

Thereafter TiO_2 nanofibers were assembled to a gas sensor by adhereing hot-pressed electrospun TiO_2 nanofibers on PCB substrate. The background of gas sensor detection performance was tested under UV illumination to investigate conductance response of the gas sensor. Conductance response of the gas sensor under UV illumination is shown in **Figure 4.14**. The gas sensor was illuminated by UV light to activate TiO_2. Under such conditions, the sensor is activated. This results in the generation of an electron and a positive hole (reaction (1)). Oxygen then accepts electron at the TiO_2 surface and becomes an oxygen ion (reaction (2)) [14-16].

$$TiO_2 \xrightarrow{h\nu} e_{cb}^- + h_{vb}^+ \quad (1)$$

$$O_{2\,(g)} + e_{cb}^- \longrightarrow O_{2\,(ads)}^- \quad (2)$$

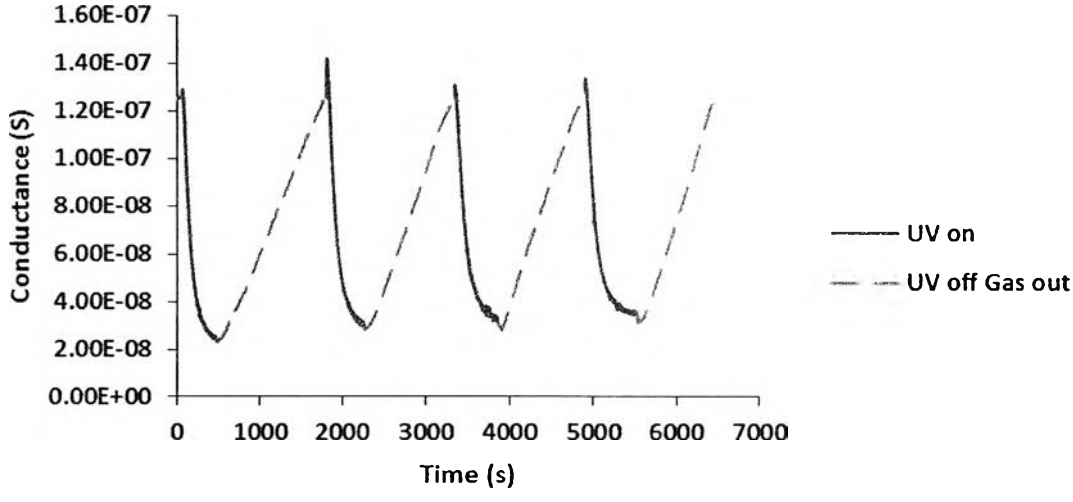

Figure 4.14 Conductance response of TiO_2 nanofiber gas sensor under UV illumination

When the UV light was turned off, a sharp decrease of conductance was observed. This decrease of conductance signal may be a result of the recombination of electron and positive hole [80, 81] which reduced the electrical conductivity of sensing materials.

Gas detection was performed after the UV light was illuminated to gas sensor, as illustrated in **Figure 4.15**. Preliminary tests were carried out using acetone and a model gas. As the target gas (acetone vapor) was injected into a chamber, a decrease in the conductance was observed. And conductance of gas sensor sharply decreased when the content of target gas increased. This phenomenon was found in acetone, methane, and methanol detection which will be further discussed in section 4.4.2. Moreover, cycle of gas detection at each content was similar to each other that gas sensor indicated the repeatability of gas detection.

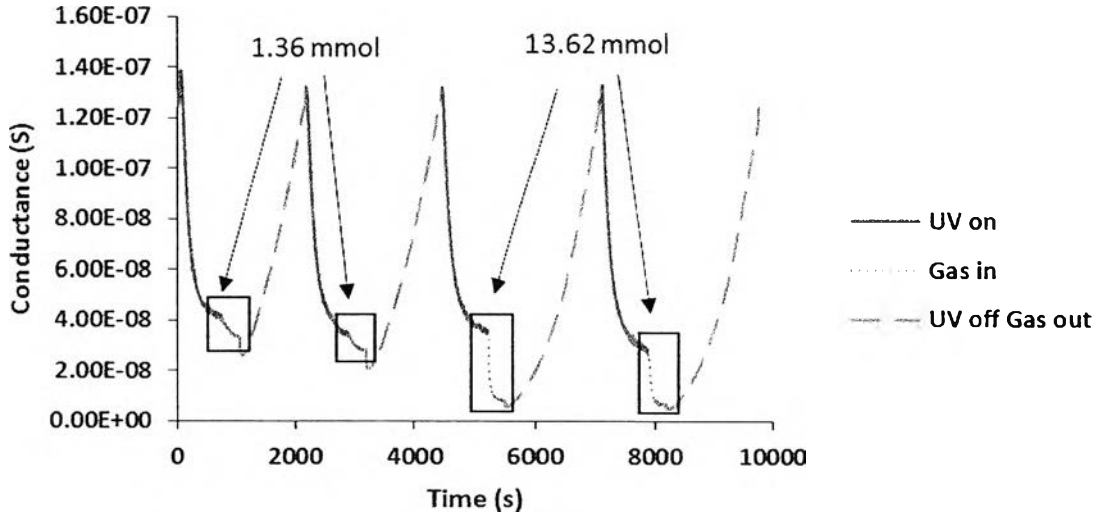

Figure 4.15 Changes in conductance responses of acetone detection using TiO_2 nanofiber gas sensor at 1.36 and 13.62 mmol of contents

4.4.2 Sensitivity of gas sensor

After TiO_2 nanofibers were fabricated into gas sensor, the sensing performance has been investigated in detection of acetone, methane, and methanol.

4.4.2.1 Acetone detection

Sensing behavior of acetone detection at 6.81 mmol is shown in **Figure** 4.16.

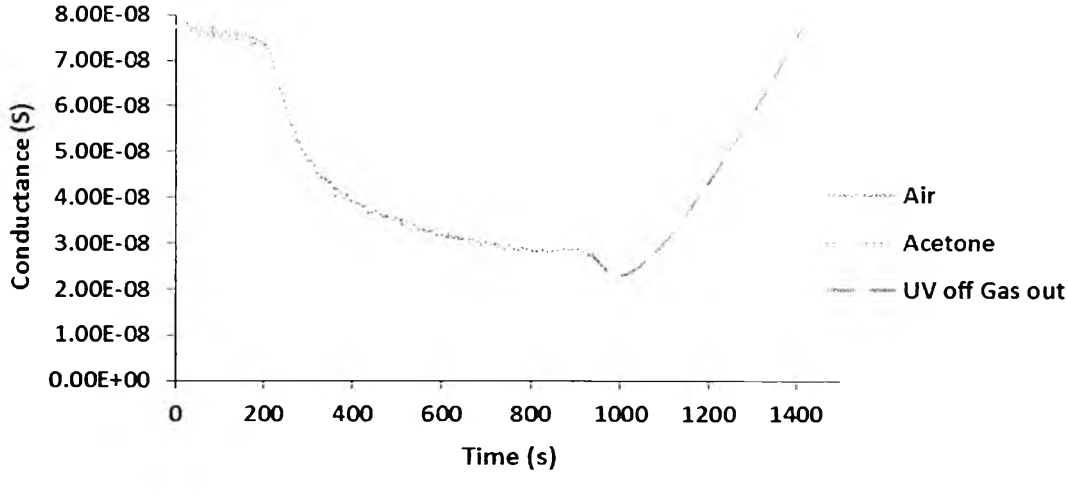

Figure 4.16 Sensing behavior of acetone detection at 6.81 mmol of TiO_2 nanofiber gas sensor

At 0 to 200 s the conductance of the gas sensor under air ambience is shown. A decrease in conductance of the gas sensor was observed when acetone was fed into the chamber at 210 s. Later on acetone was pumped out and UV light was also turned off at 935 s to recover gas sensor. The decreasing of conductance of gas sensor conforms to de Lasy Costello's [13] and Gong's [14] reports. This can be explained that when acetone was injected, acetone is oxidized into carbon dioxide, water, and hydrogen ion (reaction (3)). Hydrogen ion acts as an electron scavenger that accepts electron from TiO_2 surface and produces hydrogen gas (reaction (4)). Hence, the electrical conductance of the gas sensor is decreased.

$$CH_3COCH_{3\,(g)} + 3O_{2\,(g)} + 4h_{vb}^{+} \longrightarrow 3CO_{2\,(g)} + H_2O_{\,(g)} + 4H^{+} \quad (3)$$

$$4H^{+} + 4e_{cb}^{-} \longrightarrow 2H_{2\,(g)} \quad (4)$$

The total reaction is represented by

$$CH_3COCH_{3\,(g)} + 3O_{2\,(g)} \longrightarrow 3CO_{2\,(g)} + H_2O_{\,(g)} + 2H_{2\,(g)} \quad (5)$$

Furthermore, the response of the detection can be calculated from **Figure 4.16** and can be defined as $(G_a\text{-}G_g)/G_g$ where

G_a – Conductance of gas sensor under air ambience

G_g – Conductance of gas sensor under test gas ambience

This equation was derived from previous reports [4, 14, 23, 35]. Response of acetone detection at 6.81 mmol is found at 1.7, as shown in **Figure 4.17**.

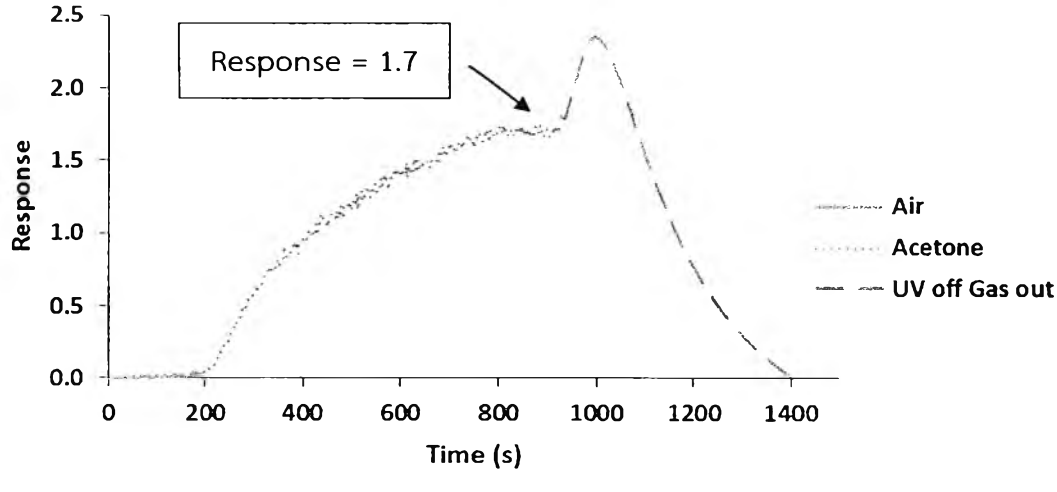

Figure 4.17 Response of acetone detection at 6.81 mmol of hot-pressed electrospun TiO_2 nanofibers

In order to investigate response of acetone at various contents, gas sensor was tested at 1.36 – 20.43 mmol of acetone contents. Response are shown in **Table 4.11** and **Figure 4.18**.

Table 4.11 Acetone detection of hot-pressed electrospun TiO_2 nanofibers at various contents

Content (mmol)	Experiment 1	2	3	Average	SD
1.36	0.32	0.35	0.31	0.32	0.02
2.72	0.72	0.73	0.71	0.71	0.02
4.09	1.03	0.97	1.02	1.00	0.03
6.81	1.85	1.66	1.68	1.73	0.10
10.90	3.03	2.76	2.71	2.73	0.17
13.62	3.65	3.39	3.76	3.60	0.19
20.43	3.74	3.39	3.70	3.61	0.19

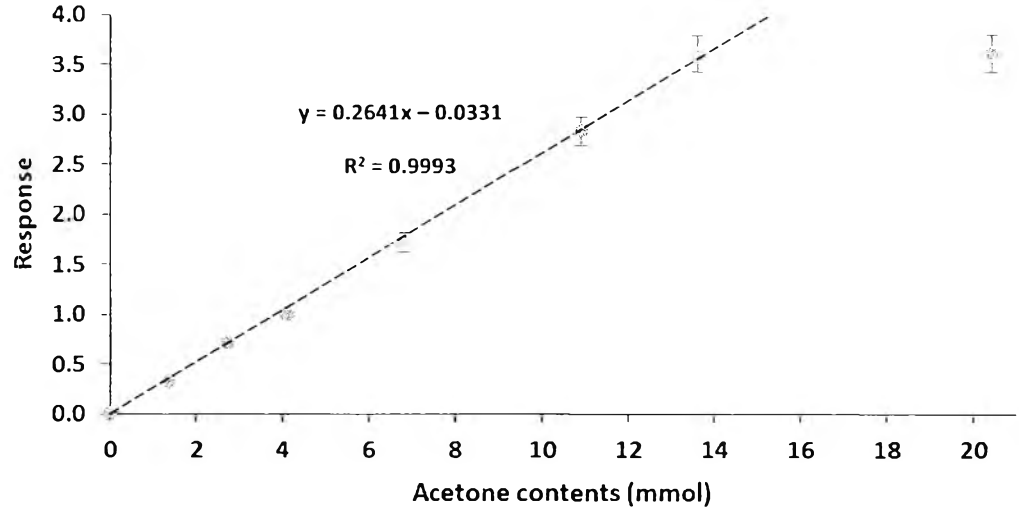

Figure 4.18 Acetone detection of hot-pressed electrospun TiO_2 nanofibers at various contents

It can be seen that as the content of acetone increased the gas sensor response also increased. The response of acetone detection is linearly proportional to acetone contents up to almost 14 mmol content. The saturation limit of this sensor is found at 13.62 mmol of acetone content as the graph has reached a plateau. Moreover, Sensitivity of gas sensor can be described through slope of calibration curve which is

0.26. Detection limit of gas sensor to acetone is estimated to be 0.24 mmol. This can be calculated from extrapolating response and the noise level of conductance baseline ($3\sigma/G_a$ where σ is standard deviation of G_a).

Additionally, the performance of the hot-pressed electrospun TiO_2 nanofibers were also compared with unpressed electrospun TiO_2 nanofibers to determine the sensitivity of gas sensing property. Unpressed electrospun TiO_2 nanofibers have been operated under the similar ambience as hot-pressed electrospun TiO_2 nanofibers, the data are shown in **Figure 4.19** and **Table 4.12**.

Table 4.12 Acetone detection of unpressed electrospun TiO_2 nanofibers at various contents

Content (mmol)	Experiment 1	2	3	Average	SD
1.36	0.29	0.22	0.41	0.31	0.10
2.72	0.62	0.57	0.49	0.56	0.07
4.09	1.08	1.02	0.81	0.97	0.15
6.81	1.04	1.47	1.15	1.22	0.22
10.90	1.69	2.05	2.65	2.13	0.48
13.62	2.06	2.46	3.07	2.53	0.51
20.43	2.12	3.07	2.89	2.69	0.50

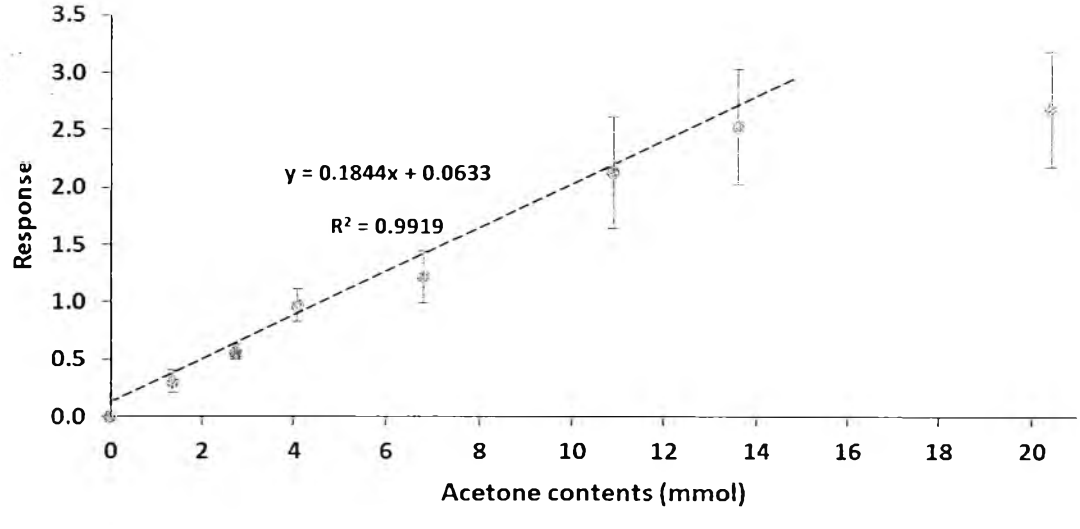

Figure 4.19 Acetone detection of unpressed electrospun TiO_2 nanofibers at various contents

Response of unpressed electrospun TiO_2 nanofibers also showed in the same trend as hot-pressed electrospun TiO_2 nanofibers which is linearly proportional to acetone contents. Sensitivity of unpressed electrospun TiO_2 nanofibers to acetone is 0.18. Detection limit of unpressed electrospun TiO_2 nanofibers to acetone is observed at 1.4 mmol. It can be seen that hot-pressed electrospun TiO_2 nanofibers exhibit higher sensitivity and detection limit than unpressed electrospun TiO_2 nanofibers. Hence, hot-pressing process can enhance surface area and surface uniformity of sensing materials which increases the sensing property of hot-pressed materials. Nevertheless, response of acetone detection is significantly different at 6.81 mmol of acetone contents, as shown in **Figure 4.20**. Furthermore, it can be seen that response of unpressed electrospun TiO_2 nanofibers exhibited more scattered response values than hot-pressed electrospun TiO_2 nanofibers. Response of gas detection via hot-pressed TiO_2 nanofibers similarly exhibit each time of detection. Therefore, hot-pressing process should be operated to enhance the uniformity of surface and the similar response of gas detection.

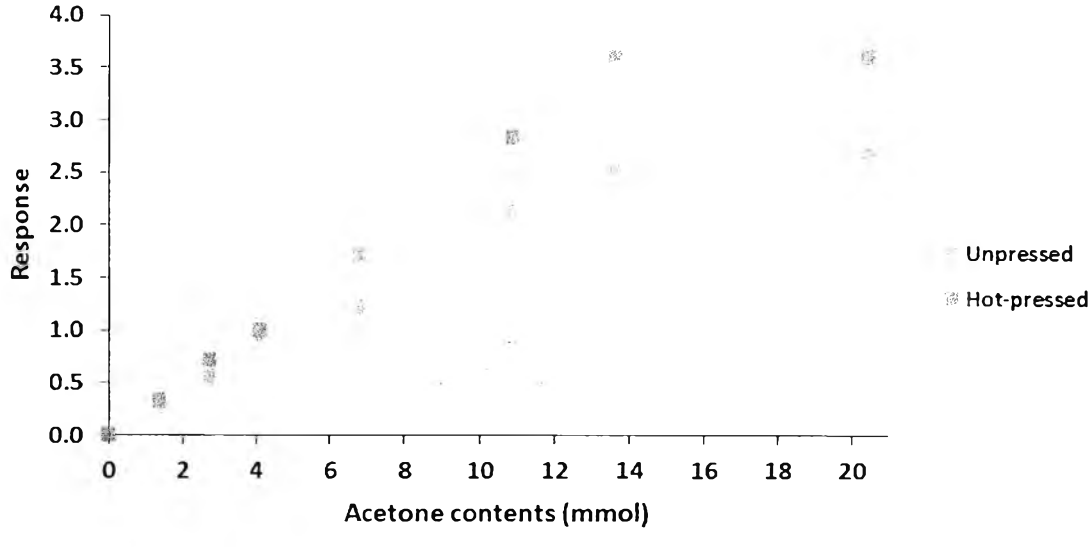

Figure 4.20 Acetone detection of unpressed and hot-pressed electrospun TiO_2 nanofibers at various contents

4.4.2.2 Methane detection

Sensing behavior of methane detection was similar to that of acetone detection where decreasing conductance of gas sensor was observed, as revealed in **Figure 4.21**.

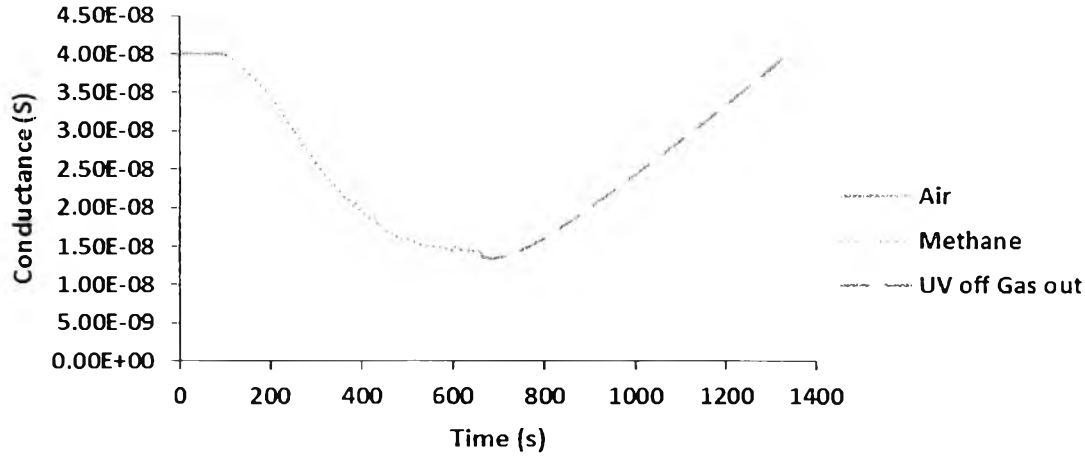

Figure 4.21 Methane detection of TiO_2 nanofiber gas sensor at 5.11 mmol

Sensing reaction of methane detection resembles to acetone detection. Methane is adsorbed on TiO_2 surface through dissociative adsorption which produces CH_3 and H on TiO_2 surface (reaction (6)).

$$2CH_{4\,(g)} \longrightarrow 2CH_{3\,(ads)} + 2H_{\,(ads)} \quad (6)$$

$$2CH_{3\,(ads)} + 2H_{\,(ads)} + 3O_{2\,(g)} + 4h_{vb}^{+} \longrightarrow 2CO_{2\,(g)} + 2H_2O_{\,(g)} + 4H^{+} \quad (7)$$

$$4H^{+} + 4e_{cb}^{-} \longrightarrow 2H_{2\,(g)} \quad (8)$$

Adsorbed molecules are oxidized into carbon dioxide, water, and hydrogen ion (reaction (7)). Hydrogen gas is generated after hydrogen ion accepts electron from TiO_2 (reaction (8)). Evidence of this reaction is not clear, however, there are a few reports [13, 82, 83] that supported this reaction. Basu *et al.* [82] postulated that dissociative adsorption of methane on metal oxide surface produced CH_3 and H on that surface. Another evidence [13] was reported by de Lasy Costello *et al.* that a GC-MS study of detection of pentane through ZnO gas sensor did not yield any product whereas alcohol functional group gave aldehyde or ketone as major product. Furthermore, it has been proposed that oxidation of organic compound occurred in the presence of air which cooperated with photo-generated hole, as mentioned in Kondarides' report [83]. Products of this reaction were CO_2 and water. Thus, sensing reaction of methane detection via gas sensor may be proposed as reaction (9)

$$2CH_{4\,(g)} + 3O_{2\,(g)} \longrightarrow 2CO_{2\,(g)} + 2H_2O_{\,(g)} + 2H_{2\,(g)} \quad (9)$$

In addition, methane detection at various contents is shown in **Table 4.13** and **Figure 4.22**.

Table 4.13 Methane detection of TiO_2 nanofiber gas sensor at various contents

Content (mmol)	Experiment 1	2	3	Average	SD
0.51	0.29	0.3	0.16	0.25	0.08
1.02	0.61	0.59	0.55	0.58	0.03
2.04	0.89	0.87	0.82	0.86	0.04
3.07	1.32	1.26	1.29	1.29	0.03
5.11	1.80	1.76	1.77	1.77	0.02
8.18	2.76	1.76	1.76	2.09	0.42
10.22	2.75	1.97	1.99	2.23	0.44
15.34	2.28	2.68	1.90	2.28	0.39

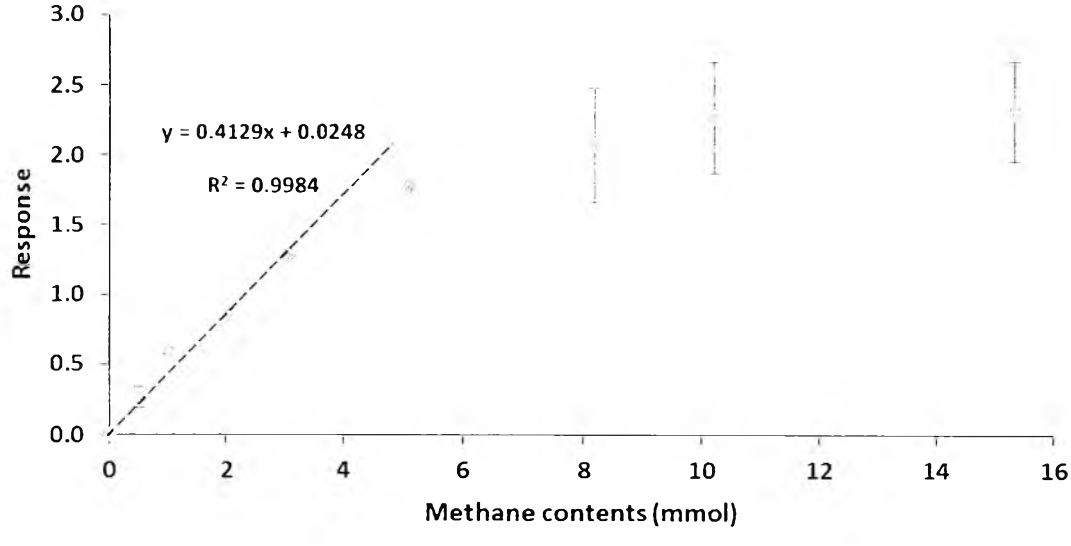

Figure 4.22 Methane detection utilizing TiO_2 nanofibers gas sensor at various contents

As shown in **Figure 4.22**, it can be seen that response and contents of methane detection are linear relationship at low content to 3.07 mmol. When the content of methane increases to 5.11 mmol, relation of response and methane contents becomes non-linear which differs from acetone detection. Sensitivity of gas sensor to methane is 0.41. Detection limit of gas sensor to methane is approximately 0.01 mmol. Saturation limit of methane detection is found at 10.22 mmol.

4.4.2.3 Methanol detection

Sensing phenomena of methanol was also similar to acetone and methane detection which is shown in **Figure 4.23**.

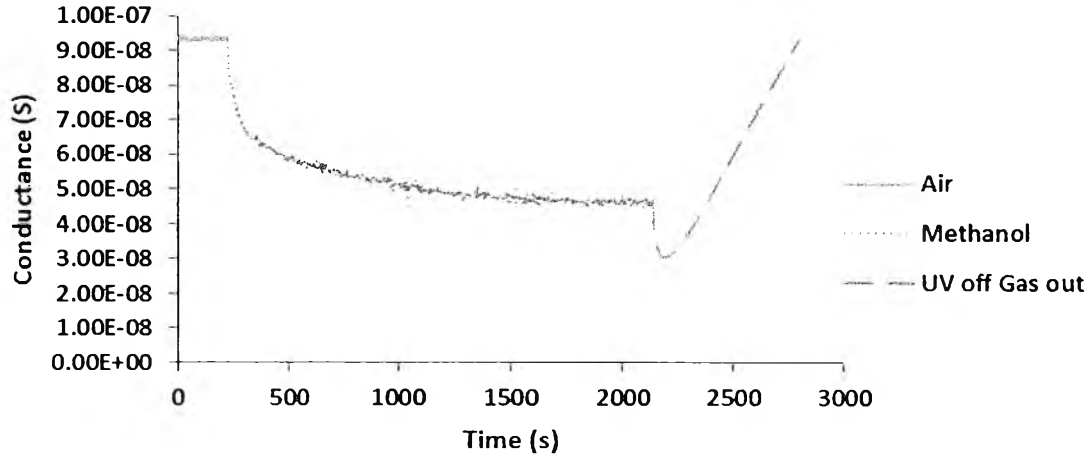

Figure 4.23 Methanol detection by TiO_2 nanofibers gas sensor at 19.77 mmol

Sensing profile in the methanol detection is also similar to acetone and methane detection. A decrease in conductance of gas sensor was observed when the content of methanol increased. Hence, sensing reaction of methanol detection can be described as

$$4CH_3OH_{(g)} + 8h_{vb}^{+} \longrightarrow 4CH_2O_{(g)} + 8H^{+} \quad (10)$$

$$4CH_2O_{(g)} + 3O_{2(g)} + 4h_{vb}^{+} \longrightarrow 4CO_{2(g)} + 2H_2O_{(g)} + 4H^{+} \quad (11)$$

$$12H^{+} + 12e_{cb}^{-} \longrightarrow 6H_{2(g)} \quad (12)$$

One difference of acetone and methane detection is in the first step of reaction (reaction (10)). Methanol brakes down via dehydrogenation reaction to yield formaldehyde, as mentioned in de Lacy Costello *et al.* [13] report. Formaldehyde is oxidized into carbon dioxide, water, and hydrogen ion (reaction (11)). Finally, hydrogen ion becomes hydrogen. This is similar to previous detection (reaction (12)).

The overall reaction of methanol detection is

$$4CH_3OH_{(g)} + 3O_{2(g)} \longrightarrow 4CO_{2(g)} + 2H_2O_{(g)} + 6H_{2(g)} \quad (13)$$

Response of methane detection at various contents is shown in **Table 4.14** and **Figure 4.24**. Sensitivity of gas sensor to methanol is 0.08. Detection limit of methanol detection is observed at 1.03 mmol. Saturation limit of methanol detection is found at 12.36 mmol.

Table 4.14 Methanol detection of TiO_2 nanofiber gas sensor at various contents

Content	Experiment			Average	SD
(mmol)	1	2	3		
2.47	0.14	0.15	0.13	0.14	0.01
4.93	0.35	0.30	0.32	0.32	0.03
7.41	0.52	0.55	0.53	0.53	0.02
12.36	1.09	0.88	1.04	1.00	0.11
19.77	0.91	0.99	1.08	0.99	0.09

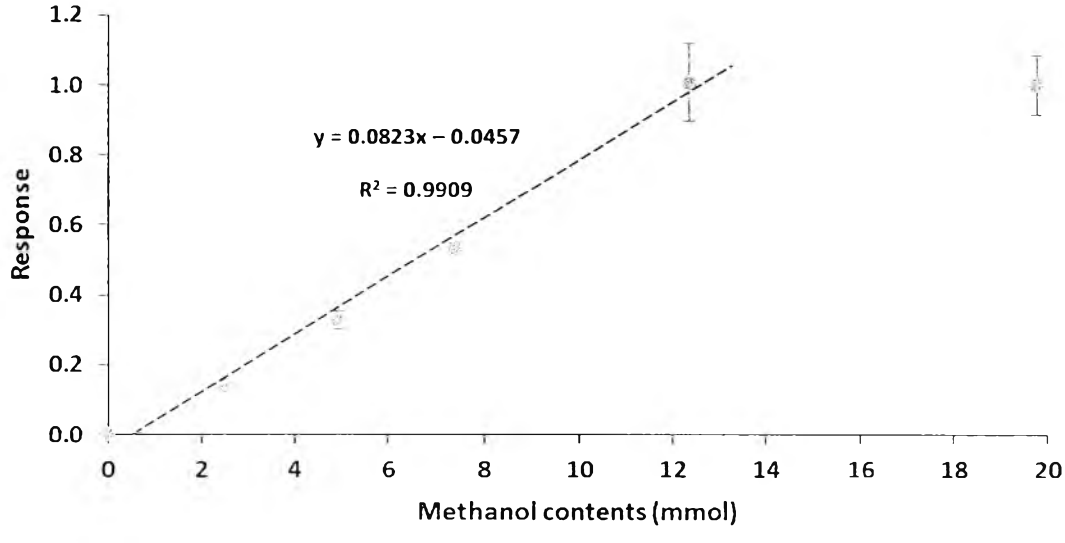

Figure 4.24 Methanol detection of TiO_2 nanofiber gas sensor at various contents

4.4.3 Selectivity of TiO_2 nanofiber gas sensor

As outlined in section 4.4.2 using the fabricated TiO_2 nanofiber gas sensor, it can be seen that target gases (acetone, methane, and methanol) can be detected in various range of contents. In order to investigate the selectivity of TiO_2 nanofiber gas sensor, response of each gases at similar content was selected to compare. At about 3 mmol of gases content, methane exhibits the highest response than acetone and methanol, as shown in **Figure 4.25**.

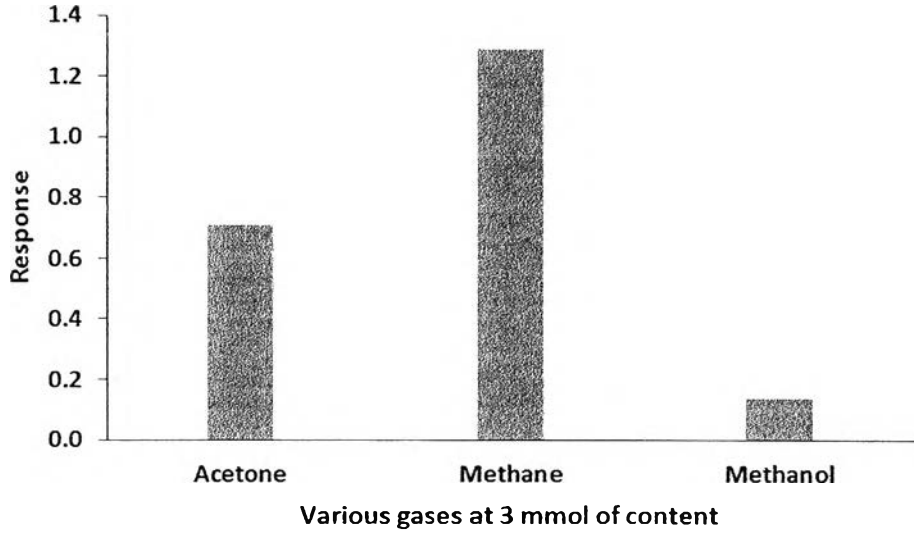

Figure 4.25 Response of acetone, methane, and methanol detection at 3 mmol of content

Due to reaction of gas detection, methanol has more reaction steps than the others. Moreover, molecular size of methane is the lowest when compared to acetone and methanol molecules. With the smaller molecular size, reaction between TiO_2 surface and methane easily occurs while that of acetone reacts more slowly due to its higher molecular size. Hence, opportunity of reaction between TiO_2 surface and acetone is less than methane. Even though methanol has the less molecular size than acetone, sensitivity of acetone is higher because of reaction steps of acetone is lower. Furthermore, this result can be predicted through the half reaction potential (E^0), as indicated in **Table 4.15**.

Table 4.15 Half reaction potential of some organic substances

Reaction	Half reaction	E^0 (V)
1	$2H^+ + 2e^- \rightleftharpoons H_{2\,(g)}$	0.00 [84]
2	$O_{2\,(g)} + 4H^+ + 4e^- \rightleftharpoons 2H_2O$	1.23 [84]
3	$CO_{2\,(g)} + 8H^+ + 8e^- \rightleftharpoons CH_{4\,(g)} + 2H_2O$	0.17 [84]
4	$3CO_{2\,(g)} + 16H^+ + 16e^- \rightleftharpoons (CH_3)_2CO + 5H_2O$	-0.13 [85]
5	$CO_{2\,(g)} + 6H^+ + 6e^- \rightleftharpoons CH_3OH + H_2O$	-0.02 [86]

Redox potential of methane reaction is the combination of half reactions 1, 2, and 3 which the overall reaction potential is 1.06 V. The combination of half reactions 1, 2,

and 4 is redox potential of acetone reaction (E^0 = 1.46 V) while methanol reaction is half reactions 1, 2, and 5 (E^0 = 1.25 V).

$$2H^+ + 2e^- \rightleftharpoons H_{2\,(g)} \qquad E^0 = 0.00\ V$$

$$O_{2\,(g)} + 4H^+ + 4e^- \rightleftharpoons 2H_2O \qquad E^0 = 1.23\ V$$

$$CO_{2\,(g)} + 8H^+ + 8e^- \rightleftharpoons CH_{4\,(g)} + 2H_2O \qquad E^0 = 0.17\ V$$

The overall reaction potential of various gases are

$$2CH_{4\,(g)} + 3O_{2\,(g)} \rightleftharpoons 2CO_{2\,(g)} + 2H_2O + 2H_{2\,(g)} \qquad E^0 = 1.06\ V$$

$$(CH_3)_2CO + 3O_{2\,(g)} \rightleftharpoons 3CO_{2\,(g)} + H_2O + 2H_{2\,(g)} \qquad E^0 = 1.46\ V$$

$$4CH_3OH + 3O_{2\,(g)} \rightleftharpoons 4CO_{2\,(g)} + 2H_2O + 6H_{2\,(g)} \qquad E^0 = 1.25\ V$$

It can be seen that redox potential of methane reaction is the lowest while the response of methane detection is higher than the others, as shown in **Figure 4.26**.

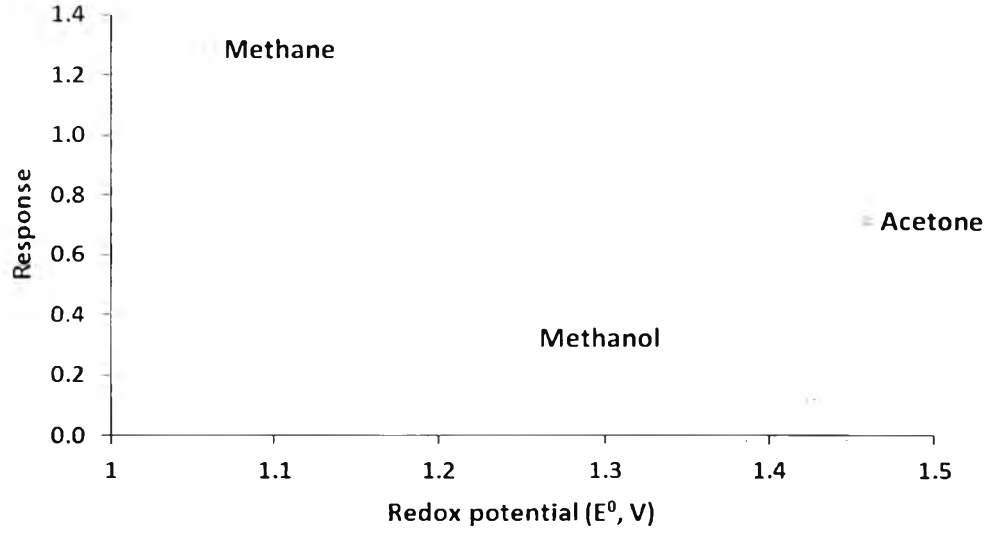

Figure 4.26 A plot of redox potential to response of various gases detection

This result may be possible that response of methane detection of gas sensor occurred from the oxidation of methane gas and the displacement of humidity in the chamber which decreased a conductance of the gas sensor. In case of polarity, methane is non-polar molecule whereas acetone and methanol are polar molecules. When methane was injected into the chamber, water molecule around the gas sensor was displaced, leading to a decrease of gas sensor conductance. Thus, detection of methane gas shows the most response between these gases. For acetone and methanol detection,

response of detection occurred through oxidation of acetone and methanol gases. Redox potential of acetone reaction is higher than methanol reaction which response of acetone detection is higher than response of methanol detection. From the previous reports [13, 14, 21], it can be seen that response of acetone detection was higher than response of methanol detection. Therefore, response of acetone and methanol detection may be generated from oxidation of acetone and methanol gases.

Nevertheless, saturation limit of methane gas is 10.23 mmol whereas saturation limit of acetone and methanol gases are 13.62 mmol and 12.36 mmol, respectively. Response of acetone gas at saturation limit content is more than both methane and methanol. This may be possible that response of methane content at the same content of acetone saturation limit (13.62 mmol) will be lower than response of acetone detection. Because response of methane detection has reached the plateau at 10.23 mmol of content. If there is an increase in content of methane, response of methane detection should be similar to response of saturation limit value, as revealed in **Figure 4.27**. Therefore, this result can be proposed that TiO_2 nanofiber gas sensor can detect the various gases in the various range of content.

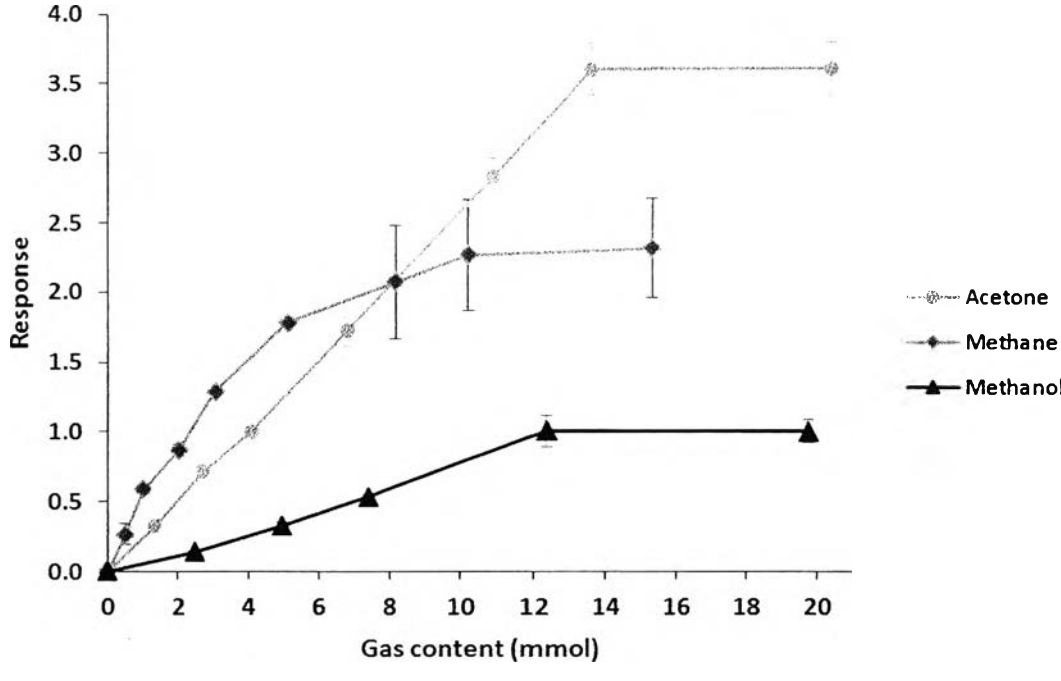

Figure 4.27 Response of TiO_2 nanofiber gas sensor under acetone, methane, and methanol detection at various contents

In addition, a gas mixture of acetone and methanol, at the content of 1.36 and 2.47 mmol respectively, were used to carry out an experiment to investigate and compare the selectivity of the sensor towards acetone and methanol detection. Response of mix gases is 0.57 that showed higher response than combination of response of acetone at 1.36 mmol and methanol at 2.47 mmol which are 0.32 and 0.14, respectively. However, response value of mix gases is between response of acetone at 4.09 mmol (0.97) and methane at 4.94 mmol (0.32), as indicated in **Figure 4.28**. Due to equality of content under detection, it can be considered that acetone exhibited more sensitive to TiO_2 nanofiber gas sensor than methanol.

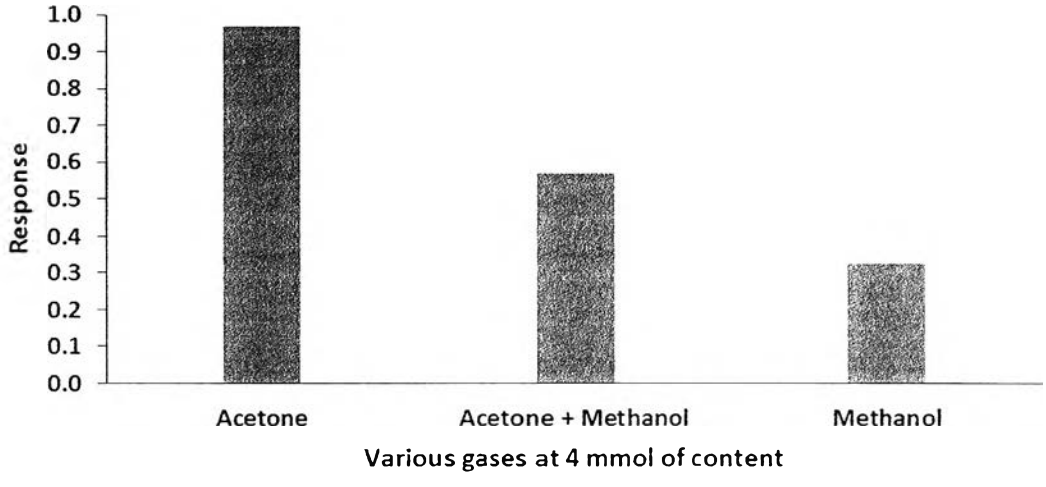

Figure 4.28 Response of TiO_2 nanofiber gas sensor under acetone, methane, and mix gases detection at 4 mmol of content

4.4.4 Stability of TiO_2 nanofiber gas sensor

As fabricated TiO_2 nanofiber gas sensor, time period of using gas sensor (life time) was measured. Life time of TiO_2 nanofiber gas sensor was investigated by measuring response of acetone at 6.81 mmol of content once a day, as shown in **Figure 4.29**.

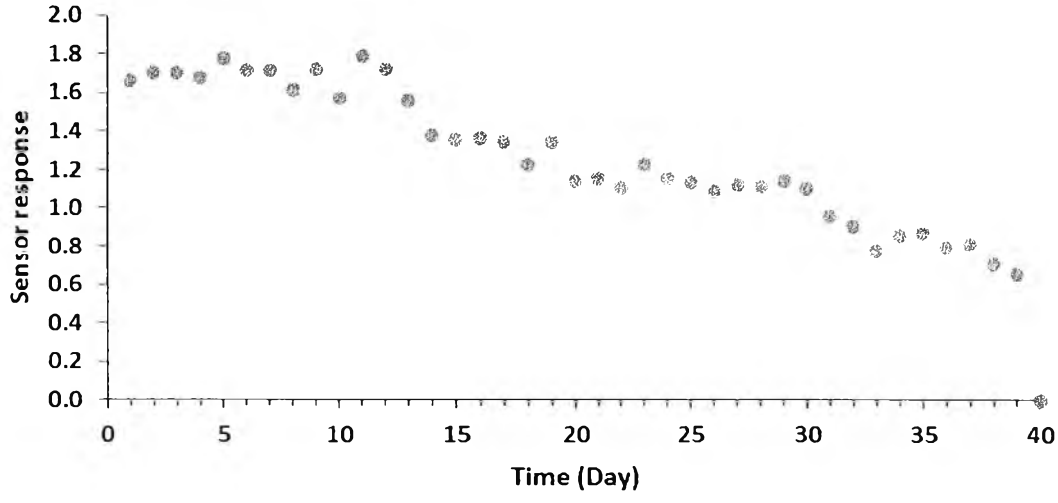

Figure 4.29 Life time of TiO_2 nanofiber gas sensor

It can be sighted that life time of gas sensor is 39 days. In 13 days, response to methane gas of gas sensor was normally observed. Response to acetone gas at 6.81 mmol decreases to about 1.4 in 14 days. Moreover, gas sensor deteriorates in 40 days. Assumption of this phenomenon is detection in high humidity ambience. Cu electrode is covered with oxide, leading to decrease in conductance of electrical signal.

4.4.5 Reproducibility of TiO_2 nanofiber gas sensor

One of many problems of sensor device is fabrication reproducibility. Most reports do not show the reproducibility in fabrication of their specimens. In our experiments, hot-pressed electrospun TiO_2 nanofiber gas sensors have been fabricated in many batches. Specimens from each batch have been put to sensing measurements in order to compare their quality and performance. It has been found that response of acetone detection through each TiO_2 nanofiber gas sensors are in range of 1.65-1.80. This result demonstrates that each of TiO_2 nanofiber gas sensors exhibit the resembling sensing performance. Hence, it can be seen that TiO_2 nanofiber gas sensors show good reproducibility, as indicated in **Figure 4.30**.

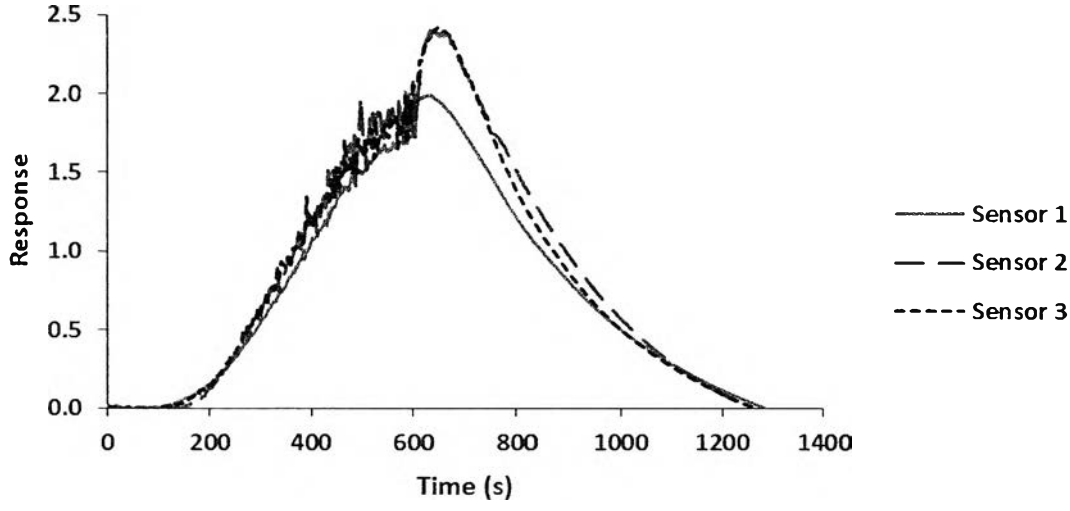

Figure 4.30 Reproducibility of gas sensor based on TiO_2 nanofibers